Soft Matter

PAPER

View Article Online
View Journal | View Issue

Cite this: *Soft Matter*, 2022, **18**, 3725

Direct and indirect effects on molecular mobility in renewable polylactide–poly(propylene adipate) block copolymers as studied *via* dielectric spectroscopy and calorimetry†

Panagiotis A. Klonos, *[ab] Zoi Terzopoulou, [a] Alexandra Zamboulis, [a] Miguel Ángel Valera, [c] Ana Mangas, [c] Apostolos Kyritsis, [b] Polycarpos Pissis [b] and Dimitrios N. Bikiaris *[a]

In this work, we study a series of sustainable block copolymers based on polylactide, PLA, and poly(propylene adipate), PPAd, both polymers being prepared from renewable resources. Envisaging a wide range of future applications in the frame of a green and circular economy, *e.g.*, packaging materials replacing conventional petrochemicals, the employment of PPAd aims at lowering the glass transition and melting temperatures of PLA and, finally, facilitation of the enzymatic degradation and compostability. The copolymers have been synthesized *via* ring opening polymerization of lactides in the presence of propylene adipate oligomers (5, 15 and 25%). The direct effects on the molecular mobility by the structure/composition are assessed in the amorphous state employing broadband dielectric spectroscopy (BDS) and calorimetry. BDS allowed the recording of local PLA and PPAd dynamics in all cases. The effects on local relaxations suggest favoring of interchain interactions, both PLA–PPAd and PPAd–PPAd. Regarding the more important segmental dynamics, the presence of PPAd leads to faster polymer chain diffusion, as monitored by the significant lowering of the dielectric and calorimetric glass transition temperature, T_g. This suggests the plasticizing role of PPAd on PLA (majority) in combination with the lowering of the average molar mass, M_n, in the copolymers from ~75 to ~30 kg mol^{-1}, which is the actual scope for the synthesis of these materials. Interestingly, a strong suppression in fragility (chain cooperativity) is additionally recorded. In contrast to calorimetry and due to the high resolving power of BDS, for the higher PPAd fraction, the weak segmental relaxation of PPAd was additionally recorded. Overall, the recordings suggest a strong increase in free volume and two individual dynamic states, one for 0 and 5% PPAd and another for 15 and 25% PPAd. Within the latter, we gained indications for partial phase nano-separation of PPAd. Regarding indirect effects, these were followed *via* crystallization. Independent of the method of crystallization, namely, melt or cold, the presence of PPAd led to the systematic lowering of crystallization and melting temperatures and enthalpies. The effects reflect the decrease of crystalline nuclei, which is confirmed by optical microscopy as in the copolymers fewer although larger crystals are formed.

Received 24th February 2022,
Accepted 13th April 2022

DOI: 10.1039/d2sm00261b

rsc.li/soft-matter-journal

1. Introduction

Polylactide (PLA) belongs to the class of aliphatic polyesters[1–4] prepared mainly by the so-called ring opening polymerization of lactide formed by lactic acid.[5] An alternative, although not that efficient, route for the synthesis of PLA is *via* the condensation of lactic acid. Lactic acid is a product of agricultural compound fermentation,[6,7] such as corn starch, potatoes, sugar cane and beet.[1,2] This has made PLA a sustainable material as well as a really good candidate for replacing the traditional petrochemicals. PLA has already found use in many different applications, from our everyday life, *e.g.*, 3D-printing[8–10] and

[a] *Department of Chemistry, Laboratory of Polymer Chemistry and Technology, Aristotle University of Thessaloniki, GR-541 24, Thessaloniki, Greece. E-mail: pklonos@central.ntua.gr, dbic@chem.auth.gr*
[b] *Department of Physics, National Technical University of Athens (NTUA), Zografou Campus, 15780, Athens, Greece*
[c] *AIMPLAS, Asociación de Investigación de Materiales Plásticos Y Conexas, Carrer de Gustave Eiffel, 4, 46980 Valencia, Spain*

† Electronic supplementary information (ESI) available. See https://doi.org/10.1039/d2sm00261b

food packaging,[4,11–13] to flame retardancy,[14] biotechnology, tissue engineering and drug delivery.[12,15–18]

PLA is a thermoplastic polymer, whereas it can exhibit two characters, *i.e.*, both amorphous, with quite poor mechanical performance,[3,19] and semicrystalline.[20–22] The presence of crystals induces severe mechanical improvements and thermal stability in PLA. What is actually wanted for processing and modern materials aiming at various applications is the wide range tuning of material performance. These are strongly connected with the polymer chain mobility/rigidity, chain entanglements and interactions as well as semicrystalline morphology.[23,24] Within the latter term two main parameters are described: the crystalline fraction, and the size and distribution of crystals throughout the polymer volume. The manipulation of semicrystalline morphology is a valuable tool for tailor-made materials and tuning properties such as the diffusion of small molecules (from oxygen and air to drugs)[25,26] or even the heat transfer.[27,28] There are many ways to modify crystallization and polymer mobility, for example, by special thermal/processing treatments, by introducing plasticizers[29] or inorganic/organic additives (*e.g.*, nanoparticles)[3,30,31] or by combining different polymers together, namely, preparing copolymers, mixtures, interpenetrating polymer networks *etc.*[13,32–34] Please note that in our days, there has been an evolving need for material synthesis, application and disposal, respecting the various environmental concerns[35–37] and, this way, following the trend for circular and green economic frame.[38,39] In connection with the latter comes the poor hydrophilicity of PLA that affects its biodegradation rate, arising from the mechanism of hydrolytic scission of the ester bonds (ref. 40 and references therein). This concerns also many of the known bio-based polyesters.[41]

A good strategy for the improvement of the properties of polyesters, accounting at the same time for the abovementioned concerns, is proved to be the synthesis of co-polyesters, for example, employing other biobased comonomers, oligomers and polymers.[34,42–45] Among the many candidates to prepare PLA-based co-polyesters, poly(*n*-alkylene adipate)s, PnAAd (with n = 2, 3, 4, 5, 6…) have been recently demonstrated.[46] These linear aliphatic polyesters are synthesized from adipic acid, which is listed by the International Energy Agency to be among the most important dicarboxylic acids, whereas it can also be prepared from renewable resources.[47] PnAAds are non-toxic and biodegradable as well, while they exhibit a high biodegradation rate and high thermal stability.[48] PnAAds are semicrystalline and their crystalline fraction can be easily tuned, by either their structure (molar mass and *n*-alkylene) or by the targeted thermal treatments.[49–53] Compared to PLA, poly(*n*-alkylene adipate)s demonstrate much easier chain diffusion, equivalently, lower glass transition temperatures (between −63 and −45 °C).[34,46,48–51] Thus, PnAAds may act as plasticizers for PLA and, simultaneously, as additional compounds that favor manipulation of crystallization.[34,44]

A recently synthesized series of block copolymers based on PLA and poly(propylene adipate), PPAd,[46] are investigated in the present work. The emphasis is on the direct effects of copolymer composition and chain length on the local and segmental molecular mobility. The said direct effects are assessed mainly in the initially amorphous state of the materials. In the last section of this work, the indirect effects of copolymer composition are studied from the point of view of polymer crystallization. The advanced technique of broadband dielectric spectroscopy (BDS)[54] is employed as the main investigation tool for molecular mobility, being a combination of differential scanning calorimetry (DSC) of the conventional as well as the temperature modulation mode (TMDSC) and polarized optical microscopy (POM). The molecular dynamics mapping for these copolymers is presented in this article for the first time, to the best of our knowledge. The results are analyzed and discussed by widely adopted routes and models, whereas we attempt the combination of the overall data and following parameters in order to gain knowledge of the realistic scenarios on the topology of the two polymers and the involvement of interchain associations.

2. Experimental

2.1. Materials

The samples investigated here are block copolymers of PLA and PPAd (*i.e.*, PLA_*b*_PPAd) with PLA/PPAd % ratios of 95/5, 85/15 and 75/25 (Fig. 1). For comparison we investigate the initial PLA. The synthesis and initial structure characterization of these systems are described in the recent work by Terzopoulou *et al.*[46] Briefly, PPAd oligomers were synthesized by the addition of pre-polymerized adipic acid *via* two stage polycondensation. The molar mass of PPAd was low and estimated as $M_n \sim 6$ kg mol^{-1}. PLA was synthesized *via* ring opening polymerization, ROP, of lactide at 180 °C. The copolymers were prepared by polymerizing L-lactide in the presence of PPAd oligomers (this diol actually being the initiator for ROP) *via* a reactive extrusion method in a torque rheometer at 180 °C. This method actually produced the development of PLA blocks on the pre-synthesized PPAd.[46] The studied samples are listed Table 1 along with values on the estimated average molar masses (M_n, M_w).

2.2. Experimental methods

2.2.1. Conventional and temperature modulation calorimetry. DSC was employed to assess the thermal transitions of PLA and its block copolymers with PPAd, in the temperature range from −110 to 200 °C, in a high purity nitrogen atmosphere (99.995%, N_2). Heat flow curves were recorded by means of a TA Q200 series DSC instrument (TA, USA), combined with a liquid nitrogen control system (LNCS), calibrated with indium for temperature and enthalpy and sapphires for heat capacity.

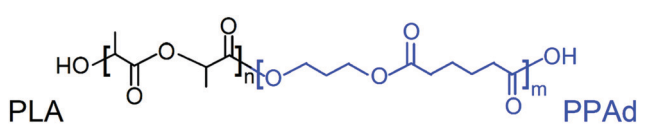

Fig. 1 Chemical structure of the copolymers under investigation, *i.e.*, consisting of PLA and PPAd blocks.

Table 1 Samples under investigation, code naming of the samples used in this article, and molar mass values (M_n, M_w) estimated in a recent work.[46]

Sample	Code name	M_n (g mol^{-1})	M_w (g mol^{-1})
PLA	PLA	76 k	120 k
PLA(95%)_*b*_PPAd (5%)	95/05	63 k	94 k
PLA(85%)_*b*_PPAd (15%)	85/15	41 k	55 k
PLA(75%)_*b*_PPAd (25%)	75/25	29 k	39 k

The measurements were performed on samples of ~8 mg in mass closed in TA aluminium Tzero pans. A first heating scan, up to 200 °C, was performed to erase thermal history and, subsequently, two main thermal protocols (Fig. S1a in the ESI†) were employed as follows: (a) standard cooling and heating at 10 K min^{-1} and (b) faster cooling to −110 °C at non-constant rate (~96 K min^{-1} in the expected range of crystallization) and heating to 200 °C at 10 K min^{-1}.

Temperature-modulation DSC measurements were also performed on all samples of about 14 mg in mass, upon melting at 190 °C, fast cooling down to −110 °C and equilibration thereafter for about 20 min. The heat capacity, c_p, was recorded upon heating at a heating rate of 2 K min^{-1} with a modulation period of 60 s and temperature amplitude of 1 K (Fig. S1b in the ESI†), in the temperature range from −110 to 180 °C.

The characteristic temperature of the glass transition step, T_g, was estimated from the heating curve as the point of half c_p elevation (TMDSC). From conventional DSC, where heat is measured directly, the half c_p (J g K^{-1}) change was nominally estimated upon normalizing the heat flow (mW) to the sample mass (mg) and heating rate (0.167 K s^{-1}). Crystallization and melting events were evaluated in terms of peak temperature maxima and enthalpy changes (ΔH in J g^{-1}).

2.2.2. Broadband dielectric spectroscopy. For the BDS measurements, the samples were melted between finely polished brass electrodes at 190 °C (Fig. 2, excellent electrical contact), forming a sandwich-like capacitor of 14 mm in diameter. Thin silica spacers were employed for that between the electrodes to preclude the electrical contact between the electrodes and keep the distance between the electrode distance (or else, the thickness of the dielectric mean) constant at ~50 μm. The complex dielectric permittivity, $\varepsilon^* = \varepsilon' - i\cdot\varepsilon''$, was recorded isothermally as a function of frequency in the range from 10^{-1} to 10^6 Hz and in the temperature range from −150 to 120 °C, in a nitrogen gas flow atmosphere, by means of a Novocontrol BDS apparatus (Novocontrol GmbH, Germany) combined with a liquid nitrogen cryogen system (Quatro). BDS is employed here for the study direct effects of copolymer composition on the molecular dynamics of PLA and PPAd, therefore, on all samples were in the initially amorphous state. This was achieved by a prior melting and a subsequent fast cooling. The dielectric permittivity was recorded upon heating in steps of 5 and 10 K.

2.2.3. Polarized optical microscopy. The POM technique was employed to examine the semicrystalline morphology. POM images were recorded during hot (or else, melt) crystallization (*i.e.*, samples melted at high temperature, 200 °C, and crystallized during the subsequent cooling, namely, suffering small supercooling), by means of a Nikon Optiphot-1 polarizing microscope equipped with a Linkam THMS 600 heated stage, a Linkam TP91 control unit and a Jenoptik Gryphax Arktur camera.

3. Results and discussion

3.1. Direct composition effects on molecular mobility (amorphous state)

3.1.1. Calorimetry. To assess the direct effects of composition on molecular dynamics we bring the sample to the amorphous state. This could be achieved by melting the samples at 200 °C and cooling at a high rate (close to 100 K min^{-1}, inset of Fig. 3). We should report that during this first heating (not shown), no endothermal peaks denoting solvents (or water) evaporation were recorded.

In Fig. 3, we present the subsequent DSC heating of the initially amorphous samples at 10 K min^{-1}. Therein, single glass transition steps are recorded in all cases in the range from −25 to 70 °C. For higher temperatures, cold crystallization exothermal peaks are recorded (between 50 and 100 °C), as a result of the vanished melt-crystallization during the prior 'fast' cooling. Finally, all samples exhibit melting of crystals *via* the recorded endothermal peaks in the range from 100 to 170 °C.

It is obvious, already from a glance on the raw data, that there are systematic changes on all thermal transitions. The single glass

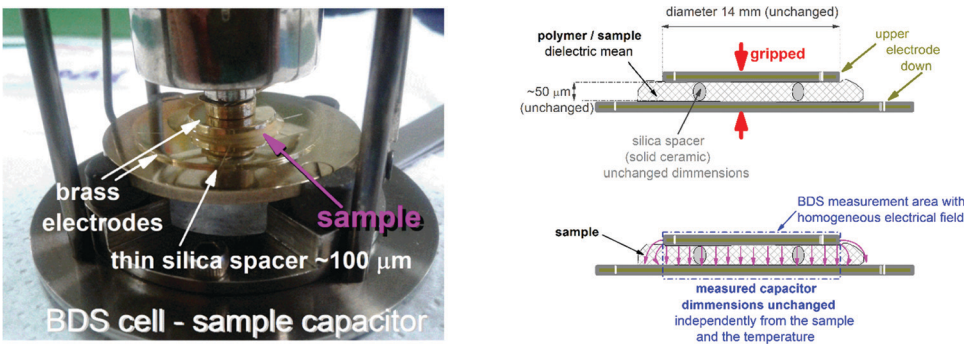

Fig. 2 Representative BDS sample in the form of electric capacitor (sandwich-like), (left) positioned in the Novocontrol BDS cell. (Right) Dimensionality of the measured sample.

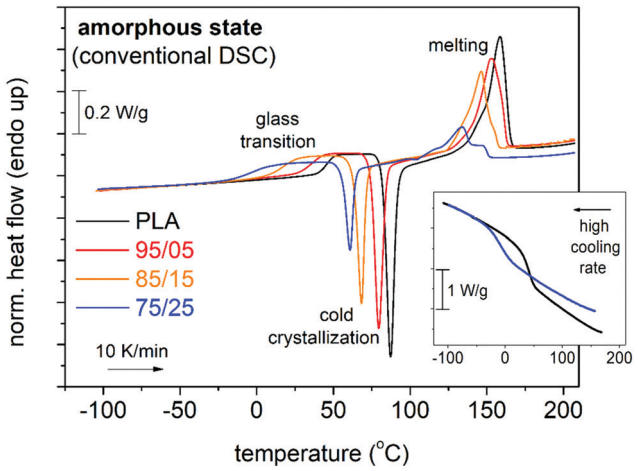

Fig. 3 Comparative DSC traces during heating at 10 K min^{-1} for all initially amorphous samples. The main thermal events are indicated on the plots. The recorded heat flow (in mW) is shown here upon normalization to each sample mass (W g^{-1}). The inset shows examples of prior cooling at a fast rate that led to eliminated crystallization of PLA and 75/25.

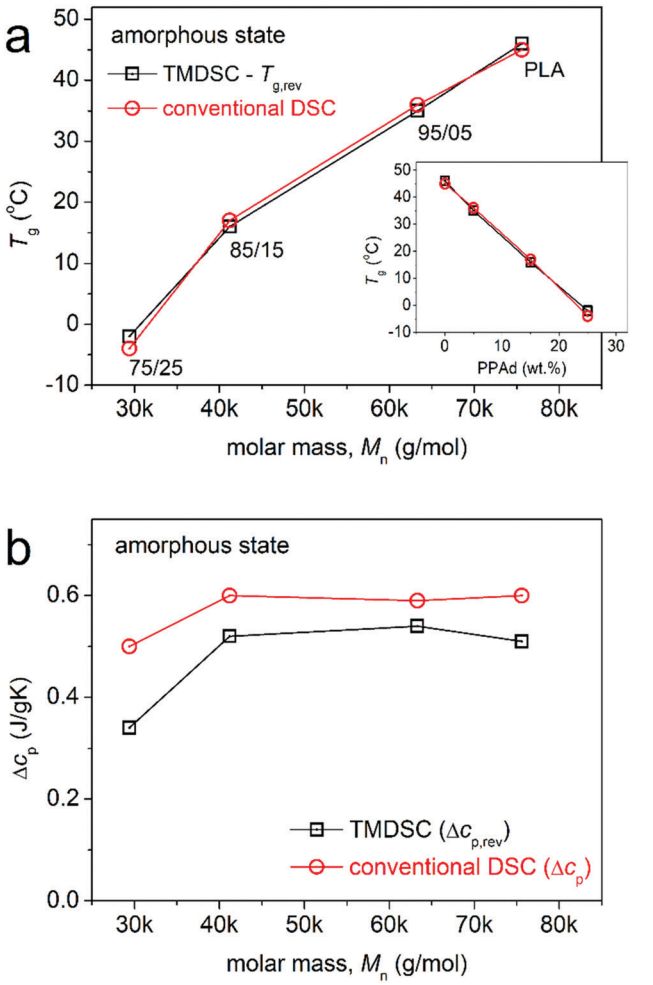

Fig. 4 The M_n (sample) dependence of (a) glass transition temperature and (b) heat capacity change during glass transition for the initially amorphous samples. In (a), the sample code names are given along the experimental point, for the sake of clarity, whereas the inset shows the PPAd wt. fraction dependence of T_g.

transition is a first strong indication for the homogeneity (miscibility)[13] of the copolymers, namely, no separation of the two polymer phases that individually demonstrate severely different glass transition temperatures. Please note that this result refers to the amorphous state (upon 'melt-quenching'). In this frame, we may report that Genovese *et al.*[13] studied polylactide-based triblock copolymers and revealed a peculiar mechanism of segregation that depends on the thermal treatment, for example, not detected in the simply quenched samples.[13]

To further study the glass transition and more accurately evaluate the corresponding heat capacity change, Δc_p, TMDSC was employed for initially amorphous samples (melted and fast cooled). The results are shown in Fig. S2 in the ESI.† The reversing part of heat capacity ($c_{p,rev}$), or else the real c_p, is actually exploited for the said evaluation and is shown in Fig. S2b (ESI†), comparatively for all samples.

The characteristic temperatures, T_g (conventional DSC) and $T_{g,rev}$ (TMDSC), were estimated employing the half Δc_p and $\Delta c_{p,rev}$ changes, respectively. The T_g values have been plotted in Fig. 4a for the four samples against their M_n. Please note that the increase of PPAd content (inset to Fig. 4a) results in a significant decrease of M_n (Table 1). In agreement between the DSC methods, T_g increases monotonically with M_n (and composition) from about −3 °C (75/25) to 46 °C (PLA). The trends suggest much faster chain mobility in the presence of PPAd. This could also suggest easier polymer chain diffusion in the sense of increased free volume and suppression of the chain-chain cooperativity, as expected, when significantly lowering the polymer chain length. However, the origins are not directly clear only by the DSC findings, namely, as to whether the easier chains diffusion arises from the shortening of the chains or the increase in free volume for other reasons. Please note that the two polymer compounds carry significant fraction of active molecular groups, namely, back bone carbonyls (both polymers), side hydroxyls (PLA) and side carboxyls (PPAd)[46] that can favor the formation of interchain interactions. These interactions are expected to hinder the chain mobility (diffusion and cooperativity) and be pronounced for shorter chains.[55–57] Coming to the strength of glass transition, the M_n dependence of Δc_p is shown in Fig. 4b. The trend of Δc_p is to increase with M_n, which is in general expected for these relatively low M_ns. The trend is, however, not expected when considering the increasing amount of the more mobile PPAd. To more clearly discuss the changes in Δc_p it is essential to perform normalization to each polymer phase weight (wt.) content. This is not straightforward for these systems, as both the wt. fractions and the chain lengths change, while at the same time there are no available data for Δc_p of PLA and PPAd homopolymers with various low M_ns. Therefore, we will attempt to shed more light on molecular mobility, in terms of time scale, cooperativity, and strength of mobilization, by BDS.

The effects on cold crystallization and melting, will be briefly discussed in the last section of this article, along with more results by DSC and POM.

3.1.2. Dielectric spectroscopy. We now proceed with BDS recordings, focusing on the imaginary part of dielectric permittivity, ε'', which is considered representative of the dielectric loss.[58] To facilitate a direct comparison with the calorimetric view (Fig. 3 and Fig. S2, ESI†), we present data for ε'' against temperature at two selected frequencies (isochronal curves) 3.16 kHz and 121 Hz in Fig. 5. We recall that the results refer to initially amorphous samples, at least at temperatures below and closely above T_g (*i.e.*, prior to the interference of cold crystallization). Therein, in the order of increasing temperature we record as peaks of ε'' the following molecular dynamics, namely, the local dynamics of PPAd (strong γ_{PPAd}), the local relaxation of PLA (β or β_{PLA}) and the segmental mobility of PPAd and PLA (α_{PPAd} and α_{PPAd}, respectively). The local relaxations originate from dipole moments arising from motions (rotations and crankshaft motions) of localized molecular groups (*e.g.*, ester groups), more details being given below along with the corresponding data by further analysis. The 'alpha' process is the dielectric analogue of the calorimetric glass transition and is considered to follow the cooperative relaxation of dipole moments perpendicular to the polymer chains.[58] Obviously, when temperature increases, the dielectric response also increases, as gradually more molecular units/groups mobilize and, thus, more dipoles contribute to the dielectric permittivity. For temperatures well above T_g, the dielectric response increases more sharply, due to the mobilization of ions throughout the rubbery polymer matrix and other interfacial polarization phenomena.[58,59]

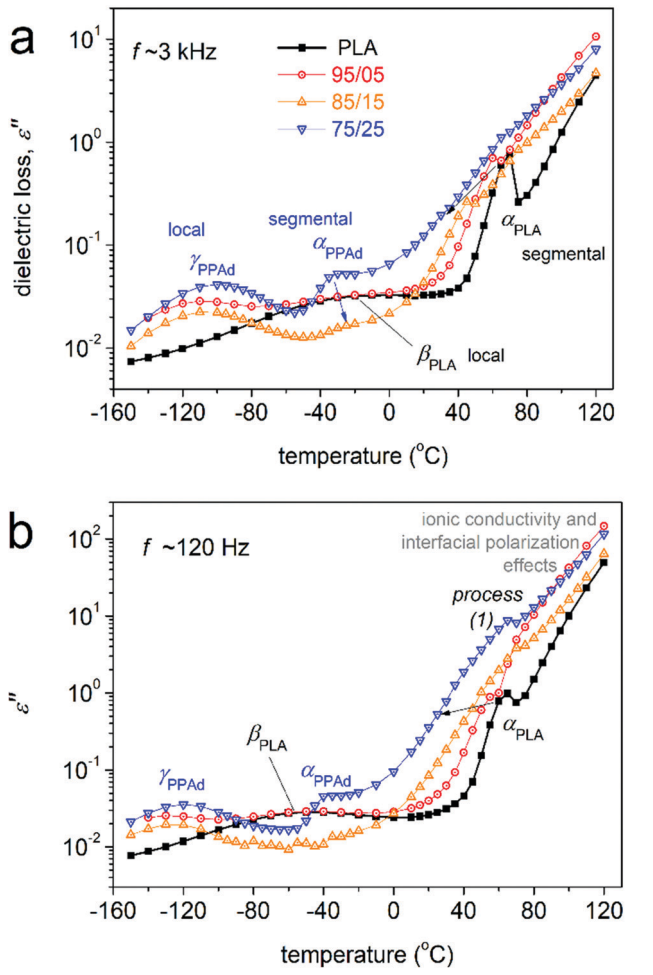

Fig. 5 Representative BDS results in terms of the comparative isochronal curves of ε'' against temperature for all samples. The results are shown for two selected frequencies (a) 3 kHz and (b) 121 Hz. Indicated are the main recorded relaxation processes (peaks of ε'').

Seeking for more details and better comparisons between the different samples, we present in Fig. S3 (ESI†) the raw BDS isothermal recordings for neat PLA (Fig. S3a, ESI†) and 75/25 (Fig. S3b, ESI†). Therein, the temperature evolutions of the recorded relaxations (peaks) are marked by added arrows. In Fig. S4, (ESI†) we show comparative isothermal $\varepsilon''(f)$ curves for all samples at fixed temperatures, in order to distinguish the direct effects of composition on each type of relaxation.

The complex dielectric data can be summarized and presented in a more efficient manner, namely, in terms of timescale and dielectric strength in a common dielectric map. To do that, and by adopting widely used methodologies, we analyzed the results of Fig. S3 and S4, by using known mathematical model functions.[58,60] Herein, the so called Havriliak–Negami, HN, function (eqn (1)) was fitted to each peak of $\varepsilon''(f)$.[61]

$$\varepsilon^*(f) = \varepsilon_\infty + \frac{\Delta\varepsilon}{[1 + (if/f_0)^{\alpha_{HN}}]^{\beta_{HN}}} \quad (1)$$

The parameters involved within eqn (1) are as follows. ε_∞ describes the value of the real part of dielectric permittivity, ε', for $f \gg f_0$, $\Delta\varepsilon$ is the dielectric strength, f_0 is a characteristic frequency related to the frequency of maximum dielectric loss, whereas α_{HN} and β_{HN} are the shape parameters of the relaxation (width and symmetry, respectively).

For the sake of brevity, we do not show examples of this fitting process and proceed directly to the demonstration of the dielectric map of Fig. 6. This map shows for all samples the reciprocal temperature dependences of $\log f_{max}$ (Fig. 6a, time scale, else called Arrhenius plots) and that of $\Delta\varepsilon$ (Fig. 6b). The left part of the figure presents the data at temperatures $T \geq T_g$, thus, dealing with segmental dynamics, whereas the right part includes data for $T \leq T_g$, focusing on the secondary (local) dynamics. In Fig. 6a, we have added the corresponding points for T_g and $T_{g,rev}$ at the appropriate equivalent frequencies, $\log f$, −2.8 and −1.8 ($\log$ Hz), for standard DSC and TMDSC, respectively. We recall that these equivalent frequencies correspond to the slow relaxation time of $\tau \sim 100$ s at T_g (assumed constant) in the conventional DSC and the 60 s period of temperature modulation in TMDSC. Also, we have marked the range of the expected T_g for various poly(*n*-alkylene adipate)s according to the literature[34,46,48–51,62] and added points on the local and segmental processes of PBAd from ref. 34.

The local γ_{PPAd} seems to screen the most localized motions of PPAd. Obviously, the process is recorded only in the PLA/PPAd copolymers and its strength increases with the fraction of PPAd (Fig. 6b). γ_{PPAd} was fitted with a symmetric HN term

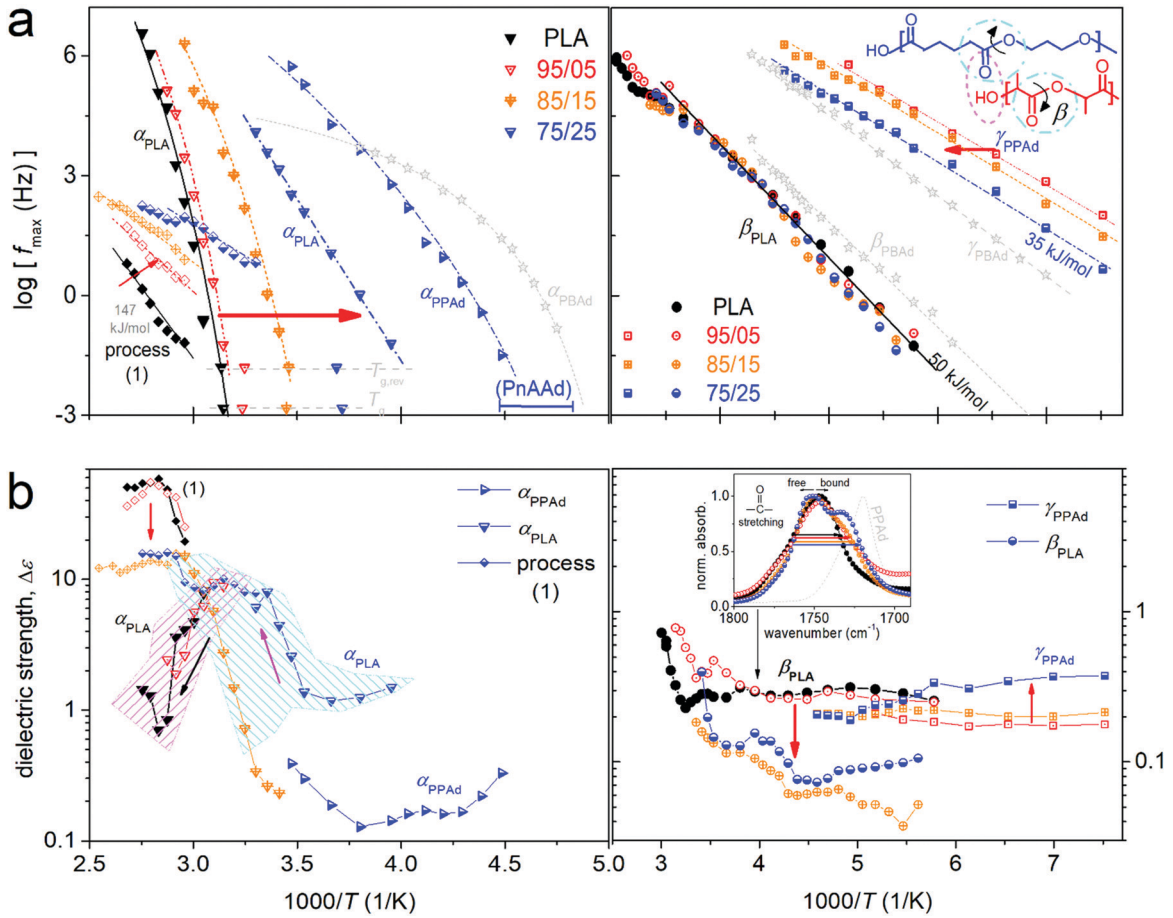

Fig. 6 Molecular mobility dielectric/calorimetric map in terms of the reciprocal dependences of (a) the log f_{max} and (b) dielectric strength, $\Delta\varepsilon$, showing the (left) segmental and (right) local dynamics, for all samples. The symbols for the different samples and relaxations are explained in (a) and (b), respectively. The added red arrows mark the effects imposed by the increasing of PPAd fraction. In (a), the added straight and curved lines connecting the experimental data points are fittings of the Arrhenius and Vogel–Fulcher–Tammann–Hesse equations, respectively, whereas, the 'star'-points correspond to BDS recordings on poly(butylene adipate), PBAd, from a previous work,[34] the calorimetric T_g points have been placed at the corresponding equivalent frequencies and, finally, the added horizontal scale bar addressed as 'PnAAd' corresponds to the T_g range of various poly(*n*-alkylene adipates). In the inset to (right - b), are infra-red spectroscopy data on the –C=O stretching for all samples (including neat PPAd). The inset of (b) has been adopted from ref. 46, with permission from MPDI, in particular form ESI† Fig S2a, employing different symbols for the different samples and slightly altered scaling.

(*i.e.*, β_{HN} = 1), relatively narrow in 75/25 (α_{HN} ~ 0.4–0.5) and wider for 85/15 and 95/05 (α_{HN} ~ 0.2–0.4), suggesting more homogenous relaxation times for increasing the PPAd amount. In general, local relaxations follow the Arrhenius law (eqn (2)).[58]

$$f(T) = f_{0,\mathrm{Arrh}} \cdot \mathrm{e}^{-\frac{E_{\mathrm{act}}}{kT}} \qquad (2)$$

In an Arrhenius behaviour of the relaxation, the activation energy, E_{act}, is constant and, thus, exhibits a linear time scale, as in our case here in Fig. 6a. E_{act} is estimated here about 35 kJ mol^{-1} and barely changes with composition. Interestingly, when increasing the amount of PPAd, γ_{PPAd} decelerates, as shown in Fig. 6a by the horizontal migration toward higher temperatures/lower frequencies. Since the literature on molecular mobility for the adipate-based polymers is still limited, we cannot definitely predict the molecular origins of γ_{PPAd}. Nevertheless, we are allowed to compare with polymers exhibiting local relaxations of a similar time scale and at the same time carrying similar or same molecular groups. In this context, we have found some resemblances between our γ_{PPAd} with a local process of poly(ethylene glycol) (γ_{PEG})[63] as well other structurally similar polymers, such as oligo-ethylene glycol methacrylates (OEGMA) and comb-like polymers based on OEGMA[64] (and references therein). The said γ_{PEG} relaxation is considered to arise from crankshaft motions of methylene sequences at the backbone of the polymer.[65,66] Such sequences exist within our PPAd, and therefore, we could propose the same origins for our γ_{PPAd}. A similar situation was recently recorded within poly(butylene adipate).[34] It is also worth recalling some previous knowledge on the molecular mobility of oligo *n*-alkylene chains when the latter exist as 'side chains', for example of acrylates.[67] When the number of carbons is smaller than n ~ 10–12 their local poly-ethylene-like relaxation is fast, whereas for and $n \geq 12$ the PE-like relaxation decelerates due to promoted chain–chain associations for the longer side chains.

Coming back to the present findings, the overall effects on homogeneity and timescale provide indications for more associations between methylene sequences of PPAd, for example with neighboring adipate chains, when PPAd increases in the copolymers.

At higher temperatures, namely in the intermediate $1000/T$ range in Fig. 6, the local β_{PLA} relaxations are recorded. The E_{act} of β_{PLA} equals $\sim$50 kJ mol^{-1}. β_{PLA} relaxation originates from fluctuations or local twisting motions of the –C═O group at the backbone of PLA.[68–70] Schematically, this can be seen in the inset of Fig. 6a. The process is recorded in both neat PLA and all copolymers. Although we have not investigated neat PPAd, a local relaxation of the same molecular origins (–C═O) is expected in the copolymers. Still the literature is quite poor on these relatively new polymers. However, our hypothesis should be true, recalling data on PBAd.[34] The corresponding points on β_{PPAd} have been included in Fig. 6a and reveal a quite similar timescale to that of β_{PLA}. Regarding its shape characteristics, β_{PLA} was sufficiently fitted with a symmetric HN term of α_{HN} = 0.3 for PLA, 95/05 and 98/15 and slightly narrower for 75/25 (α_{HN} = 0.4). The dielectric strength of the process drops with the addition of PPAd in Fig. 6b. The drop is not monotonic with the PPAd amount. We believe that the strength suppression is due to the involvement of –C═O within interchain interactions. The main responsible for that are the terminal hydroxyls (–OH) of both polymer blocks (inset of Fig. 6a). The degree of this interaction (–C═O–HO–) precludes the twisting of some ester groups, which become dielectrically less active, reducing $\Delta\varepsilon$. The interaction is favored upon increase of PPAd fraction, as, simultaneously, the average chain length of copolymers drops and, expectedly, the fraction of free chain ends (–OH) increases. More direct evidence on this interaction can be seen from infrared spectroscopy data shown in a recent work.[46] These results have been adapted and included in Fig. 6b as an inset. They reveal an increasing contribution of 'bound' –C═O groups (lower wavenumber band) in the presence of PPAd. Such formalism has been employed within numerous previous cases involving polymer interactions.[31,56,57,71,72] In connection to that, Alvarez *et al.*[50] studied poly(butylene isophthalate)/poly(butylene adipate) copolymers by BDS and showed similar changes in the local relaxation of PBAd (β_{PBAd}), and moreover, assigned these changes to the chain–chain associations also related with crystallinity. Despite the said interactions, it is expected that there are still many free end-groups (hydroxyls and carboxyls), as in a previous study, the hydrophilicity of the copolymers was found to increase with PPAd (lowering of M_n) and, subsequently, so did the enzymatic hydrolysis.[46]

The focus in now turned onto segmental dynamics. In neat PLA, α_{PLA} is recorded and fitted well by an asymmetric HN term with $\alpha_{HN} \sim 0.6$ and $\beta_{HN} \sim 0.6$. As expected for cooperative dynamics, the activation energy is not constant with T, and moreover, decreases for higher T. Thus, as in most trivial cases, the time scale of α_{PLA} is well described by the so-called Vogel–Fulcher–Tammann–Hesse (VFTH) equation[73,74] (eqn (3)). Within VFTH, the pre-exponential factor $f_{0,VFTH}$ is a frequency constant varying in the range 10^{12}–10^{14} Hz, T_0 is the so-called Vogel temperature and D is the so-called fragility strength parameter.[74]

$$f(T) = f_{0,VFTH} \cdot e^{-\frac{DT_0}{T - T_0}} \quad (3)$$

Upon the fitting of eqn (3) to the experimental data (curved lines in Fig. 6a) corresponding to the amorphous sample and upon fixing $f_{0,VFTH}$ to the phonon value 10^{13} Hz,[58] we were able to evaluate the dielectric glass transition temperature, $T_{g,diel}$, (=50 °C) *via* the extrapolation of the VFTH fitted curve at the equivalent frequency of DSC ($10^{-2.8}$ Hz/100 s). Then, the fragility index of α relaxation, m_α, was estimated (=178) according to eqn (4).

$$m_\alpha = 16 + 590/D \quad (4)$$

In Fig. 6b, $\Delta\varepsilon$ of α_{PLA} exhibits the expected decreasing trend with T,[58] whereas at higher temperatures, $\Delta\varepsilon$ exhibits a sharp decrease, due to the evolution of cold crystallization. Subsequently, the process becomes symmetric and wider (β_{HN} = 1 and $\alpha_{HN} \sim$ 0.4–0.5) and the $\Delta\varepsilon(T)$ changes to an increasing trend. The latter is also expected for semicrystalline polymers, due to the gradual loosening of the constraints[75–77] imposed by the crystals of the mobile amorphous fraction. Finally, we should report that the calorimetric data on T_g come in quite good agreement with the dielectric ones in Fig. 6a.

Regarding the copolymers, in all cases an α relaxation is recorded. The time scale of the latter shows a systematic acceleration with the addition of PPAd in Fig. 6a (down-pointing triangles). At the same time the curvature of the VFTH fitting decreases. These results are evaluated in terms of $T_{g,diel}$ and m_α, and the overall data are shown in Fig. 7, comparatively for all samples. $T_{g,diel}$ exhibits a systematic decrease with the addition of PPAd and drop of M_n (acceleration of dynamics), while the fragility drops gradually from 178 to 147 to 107 and to 0. The latter effect suggests the drop of cooperativity (95/05 and 85/15) to the extreme case of vanished cooperativity (75/25). In terms of size/scale, this suggests that either the cooperativity length increases dramatically[78,79] or, else, the distances between the neighboring (cooperating) polymer chains increases. This change is accompanied by the fact that the α relaxation in the copolymers has changed to 'symmetric' ($\alpha_{HN} \sim$ 0.5–0.6, β_{HN} = 1). In Fig. 6b, the $\Delta\varepsilon(T)$ trends are also different. In particular, for PLA and 95/05 $\Delta\varepsilon(T)$ is decreasing, whereas for 85/15 and 75/25 $\Delta\varepsilon(T)$ is increasing. The first case is indicative of non-constrained dynamics while the second suggests constraints that are gradually erased or loosened with T. Interestingly, this categorization regarding α relaxation coincides with a similar categorization on the suppression of $\Delta\varepsilon$ for β relaxation, noted above and is correlated with constraints due to inter-chain interactions.

Obviously, the segmental dynamics in the copolymers is strongly modified as compared to PLA. The results indicate that the α relaxation in the copolymers does not arise purely from PLA chains gathered in separate nanodomains and this is an indirect proof for a well-formed copolymeric structure. Therefore, we may conclude the existence of a situation that

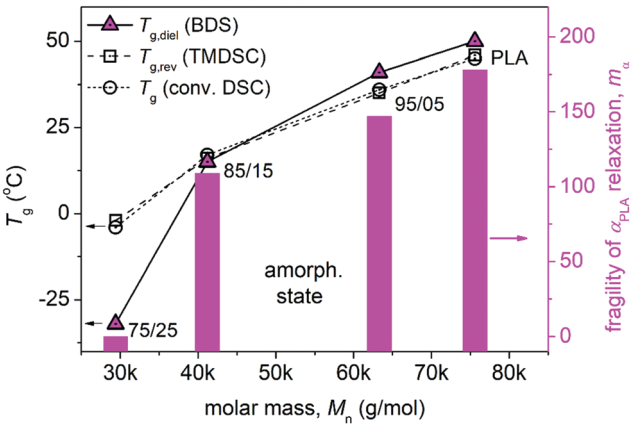

Fig. 7 The molar mass (sample) dependence of (left axis) of the dielectric and calorimetric T_g against (right axis) the fragility index of α_{PLA} relaxation, m_α. The values correspond to the amorphous state, namely, prior to cold crystallization.

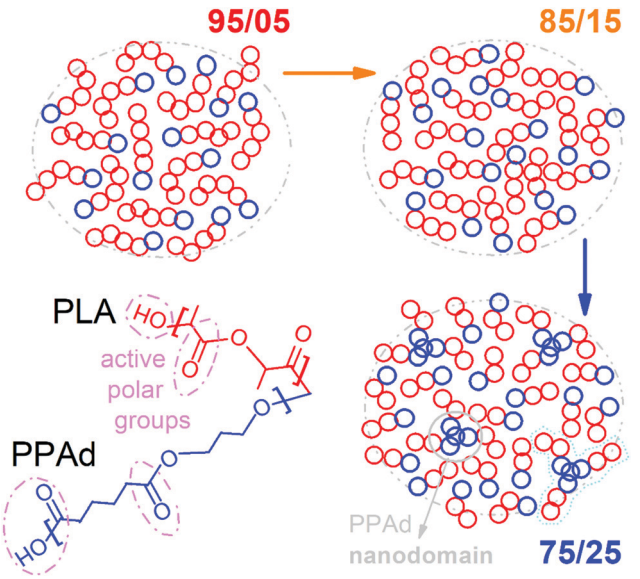

Scheme 1 Simplified schematics model for the distribution of PLA and PPAd in the copolymers, considering the overall findings by the present work.

is schematically described in Scheme 1. The copolymers are quite homogeneous systems, coming from successful synthesis. The increase in the PPAd amount, results in increasing in the inter-chain interactions and, in shorter, thus, more mobile chains which exhibit, however, significantly smaller cooperativity.

In the extreme case of 75/15, BDS was able to distinguish an additional weak process with $\alpha_{HN} \sim 0.4$ and $\beta_{HN} \sim 1$. This is shown in Fig. 6 *via* right-point triangles. The time scale of the process follows the VFTH model better, thus, denoting a level of cooperativity. The extrapolation of this coincides better with previously recorded calorimetric T_g points on various PnAAd (horizontal scale bars in Fig. 6a) and dielectric data on the alpha process of PBAd (stars in Fig. 6a).[34] Therefore, it is most likely that the process is the segmental relaxation of the PPAd phase (α_{PPAd}). Please note that in DSC no separate glass transition was recorded. The discrepancy is expected as BDS is a technique with a quite higher resolving power following *in principle* different modes (dipolar) regarding polymer chain mobility. The results suggest that in 75/25 a part of PPAd is partly formed in domains that are at least a few nanometers in size (Scheme 1). These PPAd domains should not be larger, as in no case of thermal treatment in DSC did we record the individual crystallization of PPAd. Support for that partial nano-organization of PPAd in 75/25 was supplied by scanning electron microscopy in a recent work on the same systems.[46]

Last but not least, at temperatures well above T_g, an intense signal increase is observed. Another strong ε'' peak could be resolved therein, *i.e.*, process (1). Such processes are generally related to free electrical charge transport (ions and conductivity relaxation) or phenomena related to charge accumulation at interfaces (Maxwell–Wagner–Sillars phenomenon or electrode polarization).[58,59,80] The corresponding time scale and $\Delta\varepsilon$ data have been included in Fig. 6, while the fitting shape parameters are $\beta_{HN} = 1$ and $\alpha_{HN} \sim 0.5$–0.6. In Fig. 6a, the changes in the time scale of process (1) seem to follow those of α relaxation, whereas, interestingly, $\Delta\varepsilon$ drops in general on the addition of 15 and 25% PPAd. Thus, the process is dependent on the amount and, possibly, the continuity of the PLA phase. Due to the low amount of available data, we could not safely predict the origins of the said process and, therefore, we will not comment further.

3.2. Composition effects on crystallization

We may discuss now the effects of composition on crystallization. Fig. 8 shows the DSC results for conventional cooling at 10 K min^{-1} (from the melt, Fig. 8a) and the subsequent heating (Fig. 8b). During cooling, all samples exhibit melt-crystallization peaks, mainly single with the exception of 75/25 that exhibits a double-structured peak. Expectedly, during the subsequent heating, no cold crystallization was recorded, as a result of complete crystallization–nucleation during cooling. The corresponding melting peaks are mainly single and narrow, whereas for 85/15 and 75/25 the peak is double structured.

The results of Fig. 8 have been evaluated in terms of crystallization temperatures and enthalpies, T_c and ΔH_c, respectively, and melting temperatures and enthalpies, T_m and ΔH_m, respectively. These values are presented in Fig. 9, against M_n, also comparatively with T_{cc} and ΔH_{cc}, of cold crystallization from the first DSC scan.

In Fig. 9a, both the crystallization temperatures and enthalpies increase monotonically with the increase in M_n, or else, with the decrease in PPAd. As discussed above, the effects on T_{cc} reflect the changes in nucleation more directly, whereas those of T_c (higher values) should be more representative of the rate of crystal growth, as melt-crystallization is developed without prior strong supercooling and at relatively higher temperatures (fast chain diffusion) compared to cold crystallization. In Fig. 9b, the addition of PPAd results to lower ΔH_c, ΔH_m and ΔH_{cc}. At first thought, this should suggest a drop in

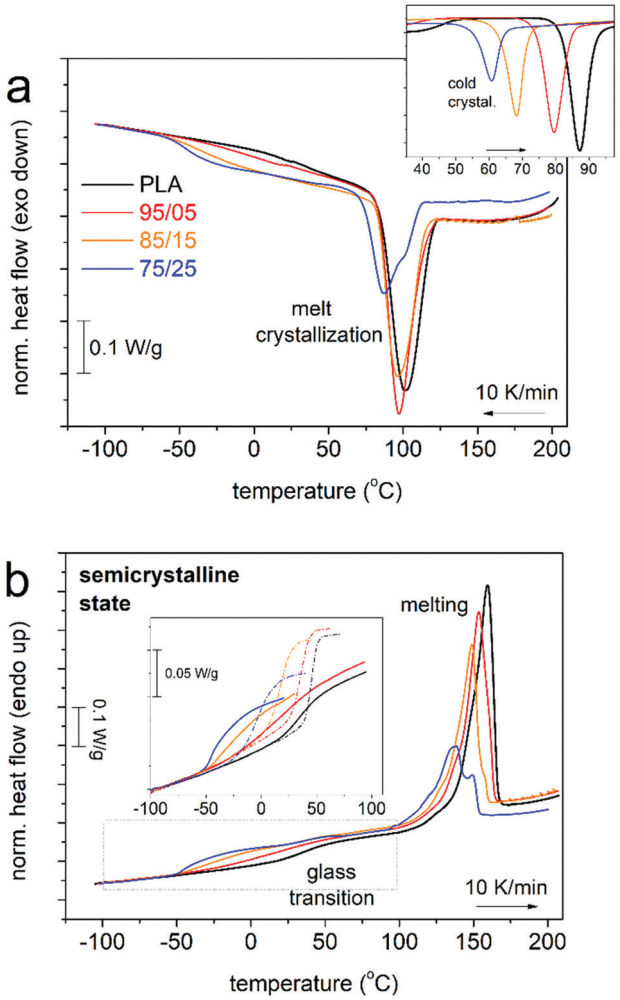

Fig. 8 (a) Comparative DSC traces during cooling at 10 K min^{-1}, demonstrating the effects on melt-crystallization for all compositions. The inset shows the results on 'cold' crystallization from the previous scan on the initially amorphous samples. (b) Comparative DSC traces during subsequent heating at 10 K min^{-1}. The heat flow is shown upon normalization to the mass of the sample. Details of the glass transition during heating are shown in the inset of (b), within which results of the amorphous samples are included for comparison (dashed–dotted lines, vertically translated for the baseline coincidence at low temperatures).

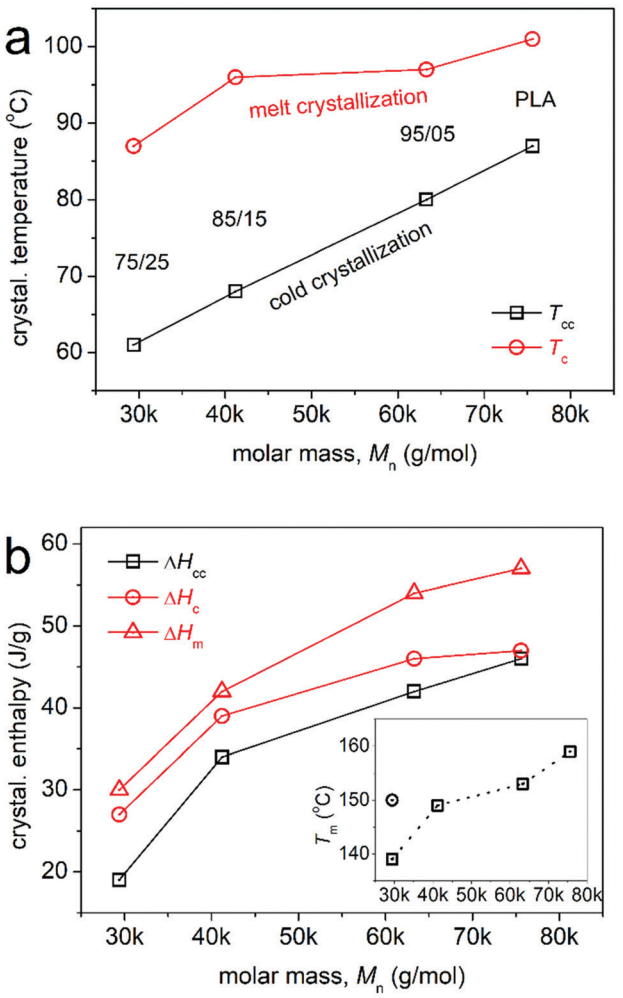

Fig. 9 (a) The M_n dependence of crystallization temperatures, T_{cc} and T_c, the corresponding sample code names being included along the experimental points. (b) The M_n dependence of crystallization, ΔH_{cc} and ΔH_c, and melting, ΔH_m, enthalpies. The inset of (b) shows the corresponding values of the melting temperature(s).

the degree of crystallinity (crystalline fraction). To more safely conclude that, the enthalpy change values should be suitably normalized[21,51] to the corresponding polymer wt. fraction. This cannot be securely done here, due to the copolymeric structuring of our systems, consisting of two polymers that individually crystallize at very different temperatures; moreover, it is yet not clear as to whether part(s) of the copolymer chains or the overall chains participate in the crystallization process. Finely, the suppression of the enthalpy is also accompanied by a suppression in T_m. This indicates the drop in the quality of crystals. The term bad quality usually reflects lower density of lamellae[81] or, in particular cases, much smaller crystallites.[31,57] Information on the degree of crystallization as well as on the crystal quality can be better evaluated by suitable experiments *via* X-ray diffraction and analysis.

In conclusion, the DSC results suggest that the addition of PPAd (or the decrease in M_n) lead to less nucleation, thus, fewer crystals of worse density or/and smaller size. To check this scenario, we employed the more direct method of POM. In Fig. 10 we present POM micrographs for different stages of melt crystallization for all samples. The data show a smaller number of crystals formed in the presence of PPAd, confirming the above mentioned suppressed nucleation. On the other hand, as in PLA the polymer volume is 'filled' with spherulites also for the copolymers, which demonstrate larger crystals as compared to neat PLA. Taking into account together the lowering of $\Delta H_{c/m}$ and T_m with the addition of PPAd and the larger crystals observed by POM, we may conclude 'indirectly' the lowering of the crystal density in the copolymers.

Finally, it is worth mentioning another exceptional behavior. In the inset to Fig. 8b, we show a focus on the glass transition region for the melt-crystallized samples (solid lines). Along with these data, we added for comparison the glass transition results

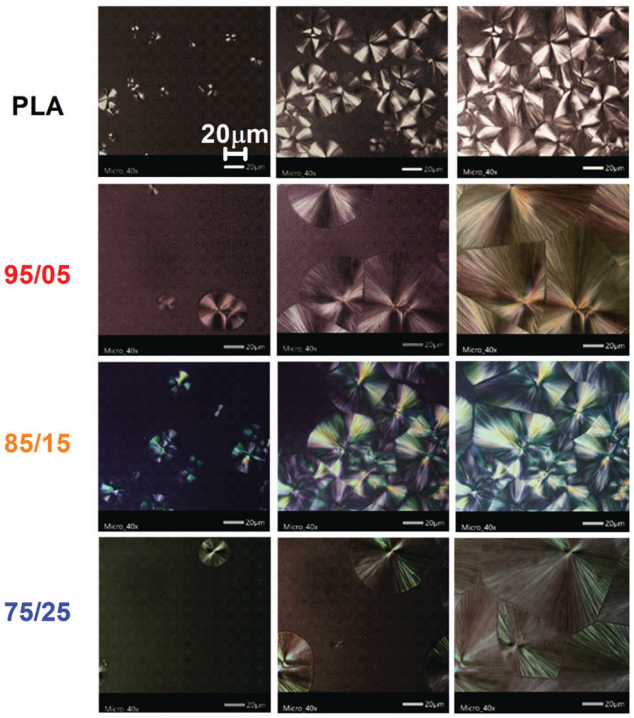

Fig. 10 POM micrographs for all samples suffered melt crystallization, the results being shown for initial, intermediate and final states of crystallization.

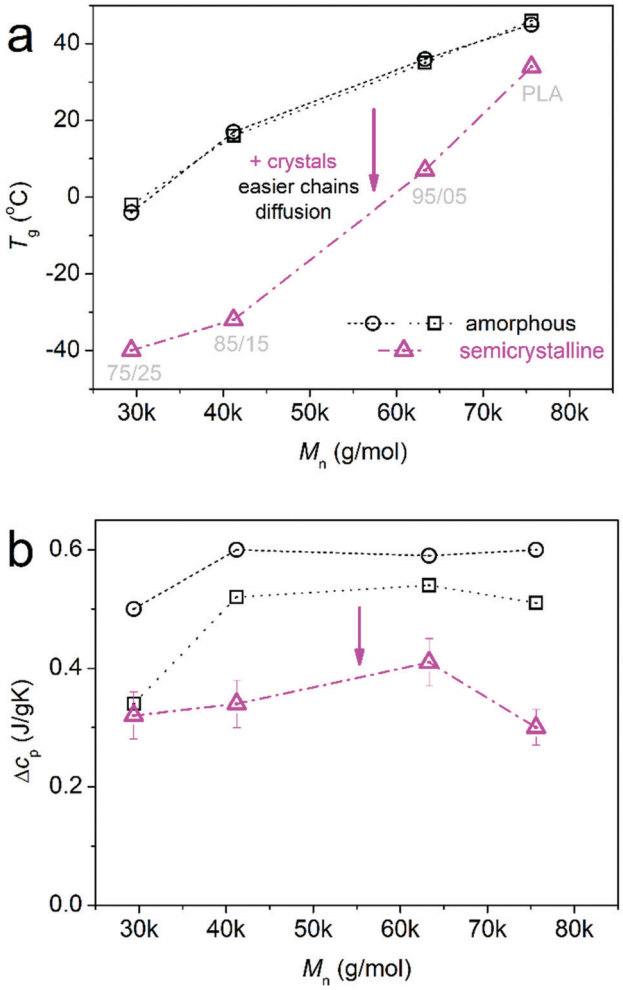

Fig. 11 The sample (M_n) dependence of (a) T_g and (b) Δc_p, as changed from the amorphous (squares – TMDSC, circles – DSC) to the semicrystalline state (up-triangles – DSC).

of the amorphous samples (dashed–dotted lines) from Fig. 3. Strikingly, upon crystallization, T_g decreases for all samples (Fig. 11a). In general, the presence of crystals is expected to hinder the polymer chain diffusion, thus, to elevate T_g. This is mainly a true fact in homopolymers.[82,83] In Fig. 11b, the effect on the glass transition strength, *i.e.*, on the Δc_p, is the expected suppression upon crystallization, as a significant fraction of the initially amorphous mobile polymer chains (amorphous Δc_p) have become rigid within the crystals. Coming again to the T_g, when directly comparing the change in T_g with the change in ΔH (Fig. 9b), we observe the controversial effect. The maximum change in the T_g occurs for the minimum increase in ΔH and the larger amount of PPAd. This suggests that the role of crystals is most possibly indirect, as actually the formation of crystals leads to further plasticization, or else, an increase in the free volume. This is favoured, again, for the lower M_ns and fewer crystals. This point is quite interesting, from the basic research point of view, and is worth being followed in a future study. For the time being, only speculations can be made to rationalize this exceptional behaviour, for example *via* a scenario involving special organization[84,85] of the polymer chains upon crystallization, favoured by the presence of PPAd.

Interesting and non-trivial effects were revealed in this work on the molecular mobility of PLA/PPAd copolymers. BDS and the critical analysis employed were proved quite powerful tools on understanding and partly rationalizing the structure–mobility relationship here. Despite these, some questions have opened regarding the structure, namely on partial nano-phase separation, possible self-organization, and, in next level, of the crystal structuring. These points could be further followed in future work, employing, for the amorphous and semicrystalline states small angle X-ray scattering[86–88] to illuminate any phase separation, XRD upon targeted thermal treatments to evaluate the degree of crystallinity and investigate alternation on the crystal/lamellar density and to further investigate molecular mobility (by BDS[56] and rheology[89]) on the initially melt- and cold-crystallized systems.

4. Conclusions

In this study we investigated the molecular mobility of new PLA/PPAd block copolymers. Since both compounds are individually semicrystalline, we study the direct composition–structure effects in the amorphous state. Therein, PPAd was found to serve as a good plasticizer for PLA in the copolymers, and also, in connection to its indirect role in the reduction of the copolymer chain length. The local β dynamics arising from the motion of the ester group (C═O), a common group in both PLA and PPAd, was found to barely change in terms of time scale.

Nevertheless, due to expected interactions between the said group and the terminal polar groups (hydroxyls and carboxyls) the dielectric strength of the local relaxation was significantly reduced, especially for the higher PPAd contents. This is also due to the increase in the fraction of chain ends for the shorter copolymer chains. A faster local mobility was recorded (γ relaxation) and was assigned to the most localized molecular motions of PPAd. The said process was found to accelerate when increasing the PLA content. The most important results refer, as expected, to segmental dynamics. This was followed *via* the so called α relaxation, the dielectric analogue of glass transition. At the increase of PPAd and lowering of M_n, α relaxation was found to strongly accelerate and exhibiting severely suppressed fragility, denoting increase of cooperativity length or/and dissociation of the relaxing chains. In other words, there seems to be extreme increase in the free volume. The existence of nanodomains of PPAd for 25% PPAd was manifested by the separated weak α_{PPAd} dynamics. Taking together the overall data on dynamics, the temperature of dielectric strength and the shape parameters, we conclude the existence of dynamically distinct behaviors between the copolymers of lower and higher PPAd contents, whereas indirect indications for special morphologies were observed. We also concluded the absence of a continuous phase of PPAd, at any composition, as manifested by the absence of individual PPAd crystallization and ionic conductivity at temperatures below T_g of the copolymers. Coming to the semicrystalline state, nucleation is suppressed in the copolymers, however, larger crystals with presumably lower density are formed. The presence of crystals resulted in the unexpected effect of further lowering of T_g, which is indicative of a non-trivial situation, arising most probably from polymer reorganization upon crystallization. Overall, the results supply evidence for the ability of wide scale manipulation of PLA (semicrystalline morphology, small molecules permeation, mechanical performance *etc.*), a polymer of high interest regarding applications as well as academia. From the methodological point of view, BDS is once again a quite powerful tool in understanding, among others, the presence of interchain interactions, the degree of chains cooperativity, in addition to indirectly shedding light on the polymers' topology, which cannot be easily assessed by microscopy.

Author contributions

Panagiotis A. Klonos: conceptualization, methodology, investigation, formal analysis, visualization, writing – original draft; Zoi Terzopoulou: investigation, formal analysis, validation, writing – review & editing; Alexandra Zamboulis: writing – review & editing; Miguel Ángel Valera: resources, validation, writing – review & editing; Ana Mangas: resources, writing – review & editing; Apostolos Kyritsis: resources, validation, writing – review & editing; Polycarpos Pissis: validation, writing – review & editing; Dimitrios Bikiaris: supervision, resources, validation, writing – review & editing.

Conflicts of interest

There are no conflicts to declare.

Acknowledgements

Panagiotis Klonos would like to acknowledge Dr Daniel Fragiadakis from the Naval Research Laboratory, Polymer Physics Section, Washington DC, USA, for kindly providing his '*grafity*' data analysis software (**https://grafitylabs.com/**).

References

1 D. Garlotta, *J. Polym. Environ.*, 2001, **9**, 63–84.
2 P. Saini, M. Arora and M. N. V. Kumar, *Adv. Drug Delivery Rev.*, 2016, **107**, 47–59.
3 S. Saeidlou, M. A. Huneault, H. Li and C. B. Park, *Prog. Polym. Sci.*, 2012, **37**, 1657–1677.
4 E. Balla, V. Daniilidis, G. Karlioti, T. Kalamas, M. Stefanidou, N. D. Bikiaris, A. Vlachopoulos, I. Koumentakou and D. N. Bikiaris, *Polymers*, 2021, **13**, 1822.
5 O. Coulembier, J. De Winter, T. Josse, L. Mespouille, P. Gerbaux and P. Dubois, *Polym. Chem.*, 2014, **5**, 2103–2108.
6 I. Armentano, N. Bitinis, E. Fortunati, S. Mattioli, N. Rescignano, R. Verdejo, M. A. Lopez-Manchado and J. M. Kenny, *Prog. Polym. Sci.*, 2013, **38**, 1720–1747.
7 R. Auras, B. Harte and S. Selke, *Macromol. Biosci.*, 2004, **4**, 835–864.
8 T. D. Ngo, A. Kashani, G. Imbalzano, K. T. Q. Nquyen and D. Hui, *Composites, Part B*, 2018, **143**, 172–196.
9 A. Constanzo, R. Spotorno, M. V. Candal, M. M. Fernández, A. J. Müller, R. S. Graham, D. Cavallo and C. McIlroy, *Addit. Manuf.*, 2020, **36**, 101415.
10 J. Dominguez-Robles, N. K. Martin, M. L. Fong, S. A. Stewart, N. J. Irwin, M. I. Rial-Hermida, R. F. Donnely and E. Larrenta, *Pharmaceutics*, 2019, **11**, 165.
11 J. Ahmed and S. K. Varshney, *Int. J. Food. Prop.*, 2011, **14**, 37–58.
12 E. Psochia, L. Papadopoulos, D. J. Gkiliopoulos, A. Francone, M.-E. Grigora, D. Tzetzis, J. Vieira de Castro, N. M. Neves, K. S. Triantafyllidis, C. M. Sotomayor Torres, N. Kehagias and D. N. Bikiaris, *Macromol*, 2021, **1**, 49–63.
13 L. Genovese, M. Soccio, N. Lotti, M. Gazzano, V. Siracusa, E. Salatelli, F. Balestra and A. Munari, *Eur. Polym. J.*, 2017, **95**, 289–303.
14 S. Bourbigot and G. Fontaine, *Polym. Chem.*, 2010, **1**, 1413–1422.
15 T. Casalini, F. Rossi, A. Castrovinci and G. Perale, *Front. Bioeng. Biotechnol.*, 2019, **7**, 259.
16 L. Sha, Z. Chen, Z. Chen, A. Zhang and Z. Yang, *Int. J. Polym. Sci.*, 2016, **2016**, 6869154.
17 B. Wang, T. Wen, X. Zhang, A. Tercjak, X. Dong, A. J. Müller, D. Wang and D. Cavallo, *Macromolecules*, 2019, **52**, 6274–6284.
18 A. Vlachopoulos, G. Karlioti, E. Balla, V. Daniilidis, T. Kalamas, M. Stefanidou, N. D. Bikiaris, E. Christodoulou, I. Koumentakou, E. Karavas and D. N. Bikiaris, *Pharmaceutics*, 2022, **14**, 359.
19 E. Kontou, M. Niaounakis and P. Georgiopoulos, *J. Appl. Polym. Sci.*, 2011, **122**, 1519–1529.

20 R. Androsch, E. Zhuravlev and C. Schick, *Polymer*, 2014, **55**, 4932–4941.
21 M. C. Righetti, M. Gazzano, M. L. Di Lorenzo and R. Androsch, *Eur. Polym. J.*, 2015, **70**, 215–220.
22 A. J. Müller, M. Ávila, G. Saenz and J. Salazar, in *Poly(lactic acid) and technology: processing, properties, additives and applications*, ed. A. Jiménez, M. Peltzer and R. Ruseckaite, RSC Publishing, 2015, RSC Polym. Chem. Series No. 12, ch. 3, pp. 66–98.
23 R. Androsch, H. M. Naeem Iqbal and C. Schick, *Polymer*, 2015, **81**, 151–158.
24 A. Toda, R. Androsch and C. Schick, *Polymer*, 2016, **91**, 239–263.
25 J. Lin, S. Shenogin and S. Nazarenko, *Polymer*, 2002, **43**, 4733–4743.
26 A. Karourani, E. G. Andriotis, K. Chachlioudaki, K. N. Kontogiannopoulos, P. A. Klonos, A. Kyritsis, E. Pavlidou, D. N. Bikiaris, D. G. Fatouros and P. Barmpalexis, *Mol. Pharmaceutics*, 2021, **18**, 4393–4414.
27 P. A. Klonos, V. Peoglos, D. N. Bikiaris and A. Kyritsis, *J. Phys. Chem. C*, 2020, **123**, 5469–5479.
28 P. A. Klonos, S. N. Tegopoulos, C. S. Koutsiara, E. Kontou, P. Pissis and A. Kyritsis, *Soft Matter*, 2019, **18**, 1813–1824.
29 H. Kang, Y. Li, M. Gong, Y. Guo, Z. Guo, Q. Fang and X. Li, *RSC Adv.*, 2018, **8**, 11643–11651.
30 J. M. Raquez, Y. Habibi, M. Murariu and P. Dubois, *Prog. Polym. Sci.*, 2013, **38**, 1504.
31 Z. Terzopoulou, P. A. Klonos, A. Kyritsis, A. Tziolas, A. Avgeropoulos, G. Z. Papageorgiou and D. N. Bikiaris, *Polymer*, 2019, **166**, 1–12.
32 M. J. Wang, S. C. Chen, K. K. Yang and Y. Z. Wang, *RSC Adv.*, 2015, **5**, 42162–42173.
33 J. K. Oh, *Soft Matter*, 2011, **7**, 5096–5108.
34 V. Karava, A. Siamidi, M. Vlachou, E. Christodoulou, A. Zamboulis, D. N. Bikiaris, A. Kyritsis and P. A. Klonos, *Soft Matter*, 2021, **17**, 2439–2453.
35 P. Pan and Y. Inoue, *Prog. Polym. Sci.*, 2009, **34**, 605–640.
36 M. Tanaka, K. Sato, E. Kitakami, S. Kobayashi, T. Hoshiba and K. Fukushima, *Polym. J.*, 2015, **47**, 114–121.
37 L. Sisti, G. Totaro and P. Marchese, *PBS makes its entrance into the family of biobased plastics*, John Wiley & Sons, Hobocan, NJ, USA, 2016.
38 M. Hong and E. Y. X. Chen, *Green Chem.*, 2017, **19**, 3692–3706.
39 W. Post, A. Susa, R. Blaauw, K. Molenveld and R. J. I. Knoop, *Polym. Rev.*, 2020, **60**, 359–388.
40 T. Beslikas, I. Gigis, V. Goulios, J. Christoforides, G. Z. Papageorgiou and D. N. Bikiaris, *Int. J. Mol. Sci.*, 2011, **12**, 6597–6618.
41 Q. Zhang, M. Song, Y. Xu, W. Wang, Z. Wang and L. Zhang, *Prog. Polym. Sci.*, 2021, **120**, 101430.
42 G. Rizis, T. G. van de Ven and A. Eisenberg, *Soft Matter*, 2014, **10**, 2825–2835.
43 J. K. Palacios, L. Zhao, N. Hadjichristidis and A. J. Müller, *Macromolecules*, 2017, **50**, 9683–9695.
44 E. Christodoulou, P. A. Klonos, K. Tsachouridis, A. Zamboulis, A. Kyritsis and D. N. Bikiaris, *Soft Matter*, 2020, **16**, 8187–8201.
45 Z. Terzopoulou, L. Papadopoulos, A. Zamboulis, D. G. Papageorgiou, G. Z. Papageorgiou and D. N. Bikiaris, *Polymers*, 2020, **12**, 1209.
46 Z. Terzopoulou, A. Zamboulis, D. N. Bikiaris, M. A. Valera and A. Mangas, *Polymers*, 2021, **13**, 4121.
47 E. Skoog, J. H. Shin, V. Saez-Jimenez, V. Mapelli and L. Olsson, *Biotechnol. Adv.*, 2018, **36**, 2248–2263.
48 T. Zorba, K. Chrissafis, K. M. Paraskevopoulos and D. N. Bikiaris, *Polym. Degrad. Stab.*, 2007, **92**, 222–230.
49 G. Z. Papageorgiou, V. Tsanaktsis and D. N. Bikiaris, *CrystEngComm*, 2014, **16**, 7963–7978.
50 C. Alvarez, M. J. Capitan, N. Lotti, A. Munari and T. A. Ezquerra, *Macromolecules*, 2003, **36**, 3245–3253.
51 M. Soccio, N. Lotti, L. Finelli, M. Gazzano and A. Munari, *Eur. Polym. J.*, 2009, **45**, 3236–3248.
52 J. Lu, Z. Li, L. Zhou, L. Wu and B. G. Li, *Polym. Degrad. Stab.*, 2019, **163**, 68–75.
53 D. Rohindra, R. Lata, K. Kuboyama and T. Ougizawa, *Polym. Cryst.*, 2019, **2**, e10037.
54 A. Schönhals and P. Szymoniak, *Dynamics of Composite Materials*, Springer, Cham, Switzerland, 2022.
55 M. E. Córdova, A. T. Lorenzo, A. J. Müller, J. N. Hoskins and S. M. Grayson, *Macromolecules*, 2011, **44**, 1742–1746.
56 P. A. Klonos, N. D. Bikiaris, E. Christodoulou, A. Zamboulis, G. Z. Papageorgiou and A. Kyritsis, *Polymer*, 2022, **242**, 124603.
57 P. A. Klonos, L. Papadopoulos, M. Kasimatis, H. Iatrou, A. Kyritsis and D. N. Bikiaris, *Macromolecules*, 2021, **54**, 1106–1119.
58 F. Kremer and F. Schönhals, *Broadband Dielectric Spectroscopy*, Springer-Verlag, Berlin, 2002.
59 R. Richert, A. Agapov and A. P. Sokolov, *J. Chem. Phys.*, 2011, **134**, 104508.
60 L. Genovese, M. Soccio, N. Lotti, A. Munari, A. Szymczyk, S. Paszkiewicz, A. Linares, A. Nogales and T. A. Ezquerra, *Phys. Chem. Chem. Phys.*, 2018, **20**, 15696–15706.
61 S. Havriliak and S. Negami, *Polymer*, 1967, **8**, 161–210.
62 S. Charlon, L. Delbreilh, E. Dargent, N. Follain, J. Soulestin and S. Marais, *Eur. Polym. J.*, 2016, **84**, 366–376.
63 P. Klonos, P. Pissis, V. M. Gun'ko, A. Kyritsis, N. V. Guzenko, E. M. Pakhlov, V. I. Zarko, W. Janusz, J. Skubiszewska-Zięba and R. Leboda, *Colloids Surf., A*, 2010, **360**, 220–231.
64 O. Vassiliadou, V. Chrysostomou, S. Pispas, P. A. Klonos and A. Kyritsis, *Soft Matter*, 2021, **17**, 1284.
65 S. Kripotou, P. Pissis, P. Sysel, V. Sindelar and V. A. Bershtein, *Polymer*, 2006, **47**, 357–366.
66 D. R. Figueroa, J. J. Fontanella, M. C. Wintersgill, J. P. Calame and C. G. Andeen, *Solid State Ionics*, 1988, **28–30**, 1023–1028.
67 M. Beiner and H. Huth, *Nat. Mater.*, 2003, **2**, 595–599.
68 J. Ren, O. Urakawa and K. Adachi, *Polymer*, 2002, **44**, 847–855.
69 E. Laredo, D. Newman, R. Pezzoli, A. J. Müller and A. Bello, *J. Polym. Sci., Part B: Polym. Phys.*, 2016, **54**, 680–691.
70 J. Leng, N. Kang, D. Y. Wang, J. Falkenhagen, A. F. Thünemann and A. Schönhals, *Macromol. Chem. Phys.*, 2017, **218**, 1700232.

71 M. Füllbrandt, P. J. Purohit and A. Schönhals, *Macromolecules*, 2013, **46**, 4626.
72 P. Krisanangkura, A. M. Packard, J. Burgher and F. D. Blum, *J. Polym. Sci., Part B: Polym. Phys.*, 2010, **48**, 1911–1918.
73 G. Tammann and W. Hesse, *Z. Anorg. Allg. Chem.*, 1926, **156**, 245–257.
74 R. Boehmer, K. Ngai, C. A. Angell and D. J. Plazek, *J. Chem. Phys.*, 1993, **99**, 4201–4209.
75 C. Alvarez, I. Šics, A. Nogales, Z. Denchev, S. S. Funari and T. A. Ezquerra, *Polymer*, 2004, **45**, 3953–3959.
76 L. Yu and P. Cebe, *J. Polym. Sci., Part B: Polym. Phys.*, 2009, **47**, 2520–2532.
77 P. Klonos, A. Kyritsis and P. Pissis, *Eur. Polym. J.*, 2015, **70**, 342–359.
78 I. Hodge, *J. Res. Natl. Inst. Stand. Technol.*, 1997, **102**, 195–205.
79 N. Delpouve, A. Saiter and E. Dargent, *Eur. Polym. J.*, 2011, **47**, 2414–2423.
80 G. Georgoussis, A. Kanapitsas, P. Pissis, Y. V. Savelyev, V. Ya Veselov and E. G. Privalko, *Eur. Polym. J.*, 2000, **36**, 1113–1126.
81 M. Safari, J. Maiz, G. Shi, D. Juanes, G. Liu, D. Wang, C. Mijangos, Á. Alegría and A. J. Müller, *Langmuir*, 2019, **35**, 15168–15179.
82 J. Dobbertin, J. Hannemann, C. Schick, M. Pötter and H. Dehne, *J. Chem. Phys.*, 1998, **108**, 9062–9068.
83 A. Wurm, M. Ismail, B. Kretzschmar, D. Pospiech and C. Schick, *Macromolecules*, 2010, **43**, 1480.
84 M. G. Wessels and A. Jayaraman, *Soft Matter*, 2019, **15**, 3987–3998.
85 E. Mygiakis, E. Glynos and G. Sakellariou, *Eur. Polym. J.*, 2021, **161**, 110857.
86 P. Szymoniak, B. R. Pauw, X. Qu and A. Schönhals, *Soft Matter*, 2020, **16**, 5406–5421.
87 P. Szymoniak, X. Qu, M. Abbasi, B. R. Pauw, S. Henning, Z. Li, D. Y. Wang, C. Schick, K. Saalwächter and A. Schönhals, *Soft Matter*, 2021, **17**, 2775–2790.
88 N. C. Murillo, P. Szymoniak, G. J. Smales, H. Sturm and A. Schönhals, *ACS Appl. Polym. Mater.*, 2021, **3**, 6572–6585.
89 Z. C. Yan, E. van Ruymbeke and D. Vlassopoulos, *Macromolecules*, 2021, **54**, 11047–11060.